Optical polarimetry: methods, instruments and calibration techniques

Andrei Berdyugin, Vilppu Piirola, and Juri Poutanen

Abstract In this chapter we present a brief summary of methods, instruments and calibration techniques used in modern astronomical polarimetry in the optical wavelengths. We describe the properties of various polarization devices and detectors used for optical broadband, imaging and spectropolarimetry, and discuss their advantages and disadvantages. The necessity of a proper calibration of the raw polarization data is emphasized and methods of the determination and subtraction of instrumental polarization are considered. We also present a few examples of high-precision measurements of optical polarization of black hole X-ray binaries and massive binary stars made with our DiPol-2 polarimeter, which allowed us to constrain the sources of optical emission in black hole X-ray binaries and measure orbital parameters of massive stellar binaries.

1 Introduction

The first measurements of polarization (in the optical wavelengths)[1] were performed by Dominique Francois Jean Arago and they date back to the first half of the 19th

Andrei Berdyugin
Department of Physics and Astronomy, 20014 University of Turku, Finland e-mail: andber@utu.fi

Vilppu Piirola
Department of Physics and Astronomy, 20014 University of Turku, Finland e-mail: piirola@utu.fi

Juri Poutanen
Department of Physics and Astronomy, 20014 University of Turku, Finland; Nordita, KTH Royal Institute of Technology and Stockholm University, Roslagstullsbacken 23, SE-10691 Stockholm, Sweden; Space Research Institute of the Russian Academy of Sciences, Profsoyuznaya str. 84/32, 117997 Moscow, Russia e-mail: juri.poutanen@utu.fi

[1] The terms *"optical light"* or *"optical wavelengths"* are usually understood as the wavelength range from 300 to 1000 nm. This is the range covered with the widely used UBVRI Johnson/ Cousins photometric systems.

century. However, optical polarimetry became a mainstream method of astrophysical observations only in the end of 1960s. This happened due to the grown use of sensitive photoelectric detectors, such as photomultiplier tubes (PMTs) and charge coupling devices (CCDs) in optical photometry and spectroscopy.

PMTs and CCDs are able to provide a sufficient S/N for measuring optical polarization even for low fluxes received from astronomical objects. CCD cameras, which are *panoramic* or *multi-cell* detectors, are capable of measuring polarization in many elements of image or spectrum simultaneously. With the introduction of the new detectors, powerful polarization devices and new techniques of polarization measurements have been developed. Currently, optical polarimetry is a well established observational tool, widely used on small and large optical telescopes for studying a large variety of astrophysical objects, from planets to active galaxies. As also emphasized at the EWASS 2018 meeting, about 4000 refereed publications on optical polarimetry have been published since year 2000.

1.1 Description of Polarization: Stokes Parameters, Linear and Circular Polarization

Polarization can be described by the *normalized Stokes parameters* q, u and v defined as:

$$q = Q/I\,, \quad u = U/I\,, \quad v = V/I. \tag{1}$$

Here Q, U and V are the *absolute Stokes parameters*:

$$Q = I_P \cos 2\psi \cos 2\chi\,, \quad U = I_P \sin 2\psi \cos 2\chi\,, \quad V = I_P \sin 2\chi\,, \tag{2}$$

I is the total intensity of the partially polarized light and I_P is the intensity of its *elliptically* polarized fraction. The angle ψ, which is also often denoted in the literature as θ (Theta) or PA (Polarization Angle), is the *azimuthal* angle of the *polarization ellipse* (see Fig. 1). In astronomical polarimetry it is measured counterclockwise from the direction to the celestial North in the equatorial coordinate

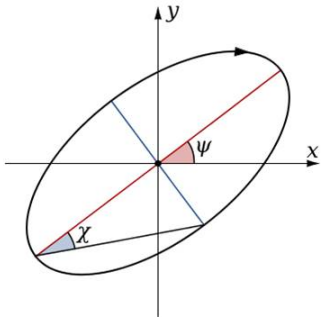

Fig. 1 Polarization ellipse of fully elliptically polarized monochromatic electromagnetic wave. This ellipse is swept by the tip of the electric vector **E** on the plane which is orthogonal to the direction of propagation. Note: in radio astronomy the magnetic vector **B** is chosen for characterization of polarization.

system. The angle χ is a measure of the *eccentricity* of the polarization ellipse, so that $\tan\chi$ is the ratio of its minor and major axes. From the normalized Stokes parameters the *degree* $P_{\rm L}$ (or $\mathrm{PD_L}$) and *direction* θ (PA) of linear polarization, and the degree of circular polarization, $P_{\rm C}$ (or $\mathrm{PD_C}$), can be found:

$$P_{\rm L} = \sqrt{q^2 + u^2}\,, \quad \theta = \frac{1}{2}\arctan\frac{u}{q}\,, \quad P_{\rm C} = v. \tag{3}$$

1.2 Mechanisms Producing Polarization of Astrophysical Objects

There are several physical processes which may be responsible for producing substantial amount of linear and/or circular polarization in the optical part of the spectrum. Those processes are:

1. Reflection of light from a solid surface (e.g. the surface of a planet or asteroid).
2. Scattering of light on free electrons, atoms, molecules or dust particles.
3. Propagation of light in the presence of the magnetic field (Zeeman and Paschen-Back effects).
4. Cyclotron and synchrotron radiation of accelerated free electrons moving in the magnetic field.
5. Interstellar polarization of distant stars due to optical dichroism of non-spherical interstellar dust grains aligned by interstellar Galactic magnetic field.

Through the processes of light emission, reflection, scattering, and absorption, optical polarimetry can provide us with important information on the properties of matter, such as spatial distribution, density, particle composition and size. It also helps us to derive the properties of stellar and interstellar magnetic fields, e.g. the field strength and geometry.

2 Polarization Modulators, Analyzers and Detectors for Optical Polarimetry

Most of optical polarimeters employ a polarization *modulator* and a polarization *analyzer*. Polarization modulator is the optical device which *modulates* the state of polarization of the incoming light beam with a given frequency. Polarization analyzer is the unit which separates the two orthogonally polarized components of light for measuring their intensities with the *detector*, synchronized with the modulation frequency.

2.1 Modulators: Retarders with Constant Phase Shift (Wave Plates)

A *retarder* is a plane parallel plate made of a uni-axial crystal cut in the way that its optical axis (the direction in which refraction index n_e is minimum) is parallel to the plate surface. The light polarized *along* this axis, moves *slower* than the light polarized in the orthogonal direction. Such plate introduces a phase shift, i.e., *retardation* τ between the orthogonally polarized components of the light beam entering the plate (Serkowski, 1974):

$$\tau = 2\pi\Delta/\lambda, \quad \Delta = (n_e - n_o)s, \tag{4}$$

where s is the thickness of the retarder, λ is the wavelength, n_e and n_o are the refractive indices for the light components polarized parallel and perpendicular to the optical axis of the crystal, respectively, and Δ is the *path difference*.

There are two types of retarders widely used in optical polarimetry: a retarder with $\tau = \pi/2$ (or $\Delta = \lambda/4$), is called *Quarter Wave Plate* (QWP), and with the $\tau = \pi$ (or $\Delta = \lambda/2$), called *Half Wave Plate* (HWP). The QWP changes the circularly polarized light with $I = V$ into linearly polarized light with $I = (Q^2 + U^2)^{1/2}$. The HWP *rotates* the plane of polarization of the linearly polarized light beam. Thus, if ϕ and θ are the directions of HWP axis and polarization of the incoming light beam measured with respect to the northern celestial pole, the direction of polarization plane of the beam emerging from the HWP becomes $2\phi - \theta$.

For a good optical retarder, the retardance should change as little as possible over the optical wavelengths. Currently available *superachromatic* optical wave plates are close to this requirement. For example, the multi-component superachromatic half and quarter wave plates offered by Bernhard Halle have the maximum deviation of retardation ±1.3% (HWP) – ±4% (QWP) and variation of the axis direction ±1.5° (QWP) – ±2.0° (HWP) over the spectral range 310–1100 nm. They are made of quartz and magnesium fluoride and available in various apertures, up to 50x50 mm. Polymer-made superachromatic wave plates offered by Astropribor closely match the optical properties of the best crystal-made retarders, although over the slightly narrower wavelength range. They are more durable and available in a larger set of apertures, up to 60 mm.

A QWP rotated in steps of 90° and placed in front of a polarization analyzer is frequently used to measure circular polarization v. A HWP rotated by steps of 22.°5 is used for linear polarization (Stokes q and u) measurements (see Section 3.1.1). Moreover, a QWP rotated with the steps of 22.°5 can be used to measure all Stokes parameters q, u and v. However, in the latter case the intensity modulation of the light beam due to linear polarization has twice smaller amplitude, which reduces the efficiency of linear polarimetry by 50% (see e.g. Serkowski, 1974).

2.2 Modulators: Retarders with Variable Phase Shift (PEMs and FLCs)

Photoelastic or Piezoelectric Modulator (PEM) is made of non-birefringent slab of material which is stressed using piezoelectric transducer at the natural slab frequency f_0. This allows to greatly reduce the power needed to sustain the standing wave in the slab. PEM operated at the base frequency f_0 acts as a $variable$ QWP introducing the periodic phase shift $\lambda/4$ between orthogonally polarized components of the incoming light beam. Placed in front of the analyzer, PEM can be used for direct measurement of circular polarization. If the PEM is driven at the frequency $2f_0$, the phase shift $\lambda/2$ is introduced and linear polarization can be directly measured. However, in the latter case, either the PEM itself or the lower section of polarimeter (below the PEM) must be rotated to two orientations separated by 45° to allow measurement of the complete set of Stokes q and u (see Kemp, 1981; Hough et al., 2006).

Nominal modulation frequencies of PEM are tens of kHz, well above fluctuations produced in the Earth's atmosphere which makes it well suitable for high-precision polarimetry. Among other advantages are the large useful aperture and possibility to use it in the fast optical beams (up to cone angles of $\leq 50°$). The PEMs for optical polarimetry are usually made of fused silica with the anti-reflecting coating optimized for the desired photometric passband.

Ferro-electric Liquid Crystal (FLC) modulators are made of a thin layer of liquid crystal material, sandwiched between two glass plates. FLCs used in optical polarimetry have a fixed $\lambda/2$ retardation with switchable orientation of the optical axis controlled by applied drive voltage. Thus, they can be used for measuring linear polarization in a way similar to that with the PEMs. The main advantage of the FLC modulator over the PEM is the nearly square-wave modulation, which makes it more efficient.

FLCs are operated at modulation frequencies in the range from hundreds of Hz to a few kHz which is fast enough to get rid of effects due to atmospheric intensity fluctuations. The FLCs are temperature sensitive devices and must be used in a temperature controlled environment to provide internal stability of the switching rate and the switching angle. The FLCs are also known for producing a large instrumental polarization from multiple internal reflections in the birefringent material between the plates. The magnitude of this polarization can be in the range of 0.1–0.3% (Bailey et al., 2015) and is highly variable with the wavelength. Special measures must be taken to properly calibrate and remove it.

Similarly to PEMs, the FLCs currently available on the market are optimised for different spectral regions. However, unlike the constant phase-shift wave plate which can be made superachromatic, the change of passband from blue to red in the polarimeter equipped with a variable phase-shift retarder requires changing the modulator unit.

2.3 Analyzers for Optical Polarimetry: Single and Double-beam Units

A single *polaroid* is probably the very first analyzer ever used in optical polarimetry. A simple polaroid is made of hematite crystals, embedded in a polymeric transparent thin film, or layered on a glass surface. Crystals are aligned in one direction. Polaroid posses a property which is called *optical dichroism*: a strong absorption of light linearly polarized in the direction parallel to the orientation of crystal axis. Thus a rotated polaroid can be used as the simplest *single-beam* analyzer for linearly polarized light.

Obvious disadvantage in using polaroid is that half of the intensity of the incoming light beam is lost. Because in the most astronomical polarimetry applications the accuracy is determined by the number of available photons, it is important to retain as much light as possible. For this reason, polaroids and other single-beam analyzers (i.e. Nicol and Glan-Thompson prisms) are rarely employed for optical polarimetry presently. However, in certain cases, the usage of polaroids can be justified, e.g. for the imaging polarimetry of extended objects (reflecting nebulae) as for example is done in the case of HST polarimeter.

A *Double-beam* analyzer, or *polarization beam-splitter*, has the advantage of splitting the incoming light beam into two orthogonally polarized beams in such a way that both of them can be measured simultaneously. Such analyzer utilizes the property found in some uniaxial crystals, which is called a *birefringence*. In these crystals the orthogonally polarized components of the electromagnetic wave travel with different speed, i.e. have different refractive indices. The birefringence degree Δn is defined as a difference between the refraction indices of the $extraordinary$ and the $ordinary$ rays $n_e - n_o$. The extraordinary (e-ray) is polarized in the direction parallel to the crystal *principal axis*, and the ordinary (o-ray) is polarized in the perpendicular direction. There are crystals with negative Δn (beryl, calcite) and positive Δn (magnesium fluoride, quartz).

2.3.1 Double-beam Polarization Analyzers for Optical Polarimetry: Plane-parallel Calcite Plate, Savart Plate and Wollaston Prism

Because a double-beam polarization analyzer is the key element in many existing optical polarimeters, is worth to mention the most important requirements which a good optical polarization beam-splitter should meet:

1. High transparency in the optical spectral range.
2. Constant birefringence Δn over the optical wavelengths.
3. No aberrations are introduced to the telescope exit pupil.
4. The same optical path length for the e and o-rays.
5. High polarization efficiency, i.e. the completely non-polarized light beam is split in two 100% orthogonally polarized beams with intensities I_e and I_o so that $I_e = I_o$.

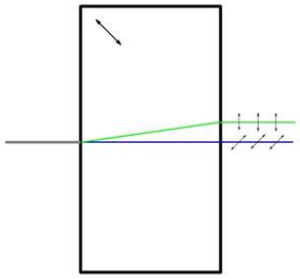

Fig. 2 Plane-parallel calcite plate. The principal axis has the angle of 45° to the plate normal. The direction of travel of the o-ray (blue) is not changed, but the e-ray (green) is shifted in the parallel direction.

There are three types of double-beam polarization analyzers most frequently used in optical broadband and spectropolarimetry. The most simple double-beam polarization analyzer is a *plane-parallel calcite plate*. It is made of calcite crystal cut parallel to the plate of cleavage (Fig. 2). Such plate splits stellar image in two by introducing a shift of the e-ray. The image separation (for $\lambda = 550$ nm) is $d = 0.109 \times h$, where h is the calcite thickness. Being simple, this polarization device can be manufactured up to the required thickness and aperture at a reasonable cost. Because it is a single-piece unit, it is not so fragile in comparison with other devices and can be handled with less caution. However, the optical path for the e and o-rays is not the same, and both images cannot be focused precisely on the same plane. Moreover, the light losses by reflection on calcite surface for the e and o-rays are different. Single calcite plate introduces a noticeable *dispersion* into the e - stellar image in the blue – near UV wavelengths. Despite of these shortcomings, the plane-parallel calcite plate is often used in applications where the image quality is not critical.

Most of the inconvenient features of a single calcite plate are avoided in *Savart plate* which is made of two plane-parallel calcite plates cemented with their principal axes at 45° to the surface normal and rotated through 90° with respect to each other (Fig. 3). Savart plate seems to be the best analyzer for the stellar polarimetry with panoramic (i.e. CCD camera) detectors. Nevertheless, accurate measurements of polarization might not be possible in crowded regions of the sky due to overlapping of the e- and o-images of the target and the nearby field stars. This problem can

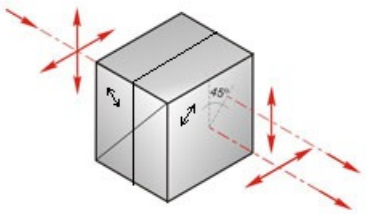

Fig. 3 Savart plate. When entering into the second crystal, the o-ray produced by first one becomes the e-ray and is displaced in the direction perpendicular to the first beam displacement. The result is two rays displaced along a diagonal. The optical path difference for the o- and e-rays is zero for normal incidence.

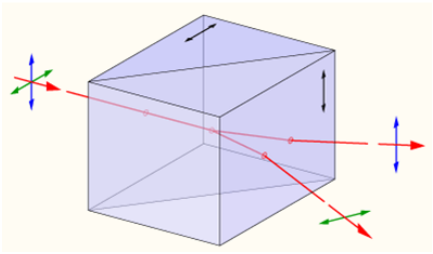

Fig. 4 Wollaston prism made of two cemented calcite wedges with orthogonally directed optical axes. The angle of separation of the o- and e-rays can be within 5° – 20°.

be solved by mounting the polarimeter on a rotator which can be turned at certain angle to change the direction of the stellar images split on the sky in a way to avoid the overlapping. Another solution is to put a stripe mask in the focal plane of the telescope, but this requires using re-imaging optics (collimator and camera lenses).

If polarimetry is done with photomultipliers, a large separation between the beams is convenient. The best double-beam analyzer which provides a large image separation and high efficiency is the *Wollaston prism*. The *two-wedged* Wollaston prism (Fig. 4) is made of two cemented (calcite) or optically contacted (quartz, magnesium fluoride) wedges with optical axes orthogonal to each other and perpendicular to the direction of propagation of the incoming light beam. The angular separation between the outgoing e- and o-rays in the Wollaston prism depends on the number of wedges N, construction angle of the outer wedges A and birefringence of material as:

$$\alpha \simeq 2 \arctan[(N-1)\ |n_o - n_e|\ \tan A]\ . \tag{5}$$

In the optical wavelengths, calcite is the preferred material, because it is transparent from 350 to 2200 nm and has a high birefringence. Thus, two-wedged calcite Wollaston prisms offered by Bernhard Halle, can provide the beam separation up to 20°. If a higher beam separation is required, the *three-wedged* calcite Wollaston prism can be used. It provides image separation up to 28° and gives the best image quality, approaching closely the ideal analyzer for the optical polarimetry (Serkowski, 1974). If a wider spectral range is needed, i.e. with the near UV and near-IR coverage, quartz or magnesium fluoride must be used. However, due to the much lower birefringence of these crystals, the beam separation is by an order of magnitude smaller. In comparison with the single calcite plate, the Wollaston prism is a more complex and expensive optical device and must be handled with care.

2.4 Detectors for Optical Polarimetry: CCDs, PMTs and APDs

There are three types of detectors used in optical polarimetry: CCD cameras, Photomultiplier Tubes (PMTs) and Avalanche Photodiodes (APDs). Each type of detector has its own advantages, disadvantages and areas of applications. There are also emerging detectors for the optical and NIR spectral ranges, namely MKIDs and

Saphira APD arrays. These are likely to play an important role in future polarimeters, particularly Saphira based systems for NIR (Finger et al., 2014).

2.4.1 Detectors for Optical Polarimetry: CCD Cameras

CCD cameras are currently the most widely used detectors for photometry and spectroscopy at the optical wavelengths. Among their main advantages are the high quantum efficiency (QE), great versatility and convenience of data acquisition. Moreover, being panoramic (multi-cell) registration devices, they are very well suited for spectroscopic and imaging applications. This feature is also very useful for *double-beam polarimetry*, because it allows us to record two orthogonally polarized stellar images or spectra simultaneously on the same detector, so that variations in atmospheric seeing and transparency will have exactly the same effect on both. Moreover, the intensity of background sky is registered automatically on the pixels surrounding stellar images and this eliminates a necessity to measure intensity and polarization of the sky separately.

The CCD cameras employed in optical polarimetry can be roughly divided into two classes: smaller units with the thermoelectric cooling and pixel area up to about 2048×2048 (used mostly for broadband polarimetry) and large pixel area (or mosaic) units with cryogenic cooling (used for spectropolarimetry, imaging polarimetry and in multi-functional instruments with optional *"polarimetry mode"*). The cameras of the first class can be connected to the computer via standard USB port used for the camera control and data acquisition. They are often equipped with the high-grade, low noise CCD detector with sensitivity optimized either for the blue-visual or visual-red spectral ranges with the maximum QE $\geq$ 90%. Many such cameras are available currently on the market at a reasonably low cost. Thus, they are well suitable for building a low-budget instrument for stellar polarimetry at the optical wavelengths. The principal design of such CCD polarimeter is shown in Fig. 5.

In broadband CCD polarimetry the data reductions can be done with *aperture photometry* method which normally includes calibration (subtraction of dark, bias and flat-fielding), sky subtraction, determination of intensities of e- and o-stellar images and converting them to the *intensity ratios* $Q_i = I_e/I_o$. The Q_i must be determined for the each orientation of the wave-plate $i = 0°, 22.^{\circ}5, 45°, ...$ The data reduction in CCD spectropolarimetry is done in the similar way: the e- and o-spectra must be extracted and, after wavelength calibration, the intensity ratios $Q_i(\lambda)$ are computed. The Stokes parameters of linear or circular polarization are obtained from the intensity ratios Q_i with the formulae given in Section 3.1.1.

The CCD detectors, while being convenient for optical polarimetry, have also some shortcomings, e.g. the relatively small full-well capacity ($\leq 200000e^-$/pixel) which results in fast pixel saturation (overexposure) of the images of the bright stars. The image download time for the small-sized CCD camera is typically around of $\simeq$1–2 s, while for the large, mosaic-type CCD detector it can be in range from few tens of seconds up to $\simeq$1 min. Thus, CCD polarimetry of bright targets, necessarily

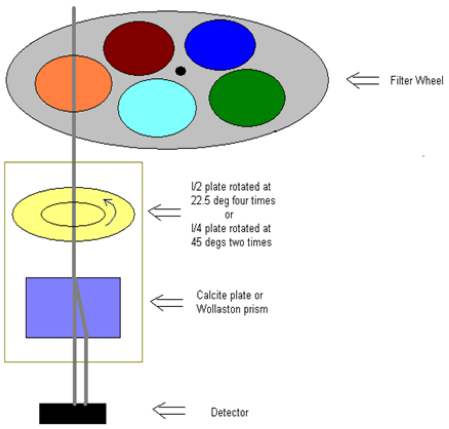

Fig. 5 The layout of the CCD optical polarimeter. Polarization components can be installed between the CCD detector and filter wheel. After passing the beam-splitting analyzer, the incoming light ray is split parallel in two orthogonally polarized rays. Instead of plane-parallel calcite shown on the figure, the other analyzer, e.g., Wollaston prism can be used.

done with short exposures, may become very inefficient, because most of the time is spent on image downloads.

The download time problem is removed in CCD cameras with *fast frame transfer*. The CCD chip in such a camera has two areas, one is for the image exposure and another for the temporal image storage. As soon as the exposure is taken, the image is swiftly shifted vertically from the exposure area into the masked storage area from where it is transferred to the camera readout register. Thus, for example, ANDOR iXon Ultra 897 EMCCD camera can provide an impressive frame rate up to 56 full-frame images/sec. Even higher frame rate is achieved in the sub-frame readout mode. The frame-transfer EMCCDs are rather expensive and available only with a relatively small pixel area, up to 1024×1024. Nevertheless, such camera can be considered as a very good option for building an efficient and versatile CCD polarimeter operating in the optical wavelengths.

2.4.2 Detectors for Optical Polarimetry: Photomultiplier Tubes

Although most of the existing astronomical polarimeters employ CCD cameras, *Photomultiplier tubes (PMTs)* are still used in optical polarimetry. The main advantages of PMTs, making them a good choice as detectors for certain applications, are the instant readout, wide dynamical range and ability to faithfully register high fluxes. Thus, a typical PMT retains linear response up to the level of $10^6 e^-$/s in the pulse counting mode and up to $\leq 10^8 e^-$/s in a direct photo-current amplification mode.

Polarimetry is a "photon hungry" observational technique. The accuracy is critically dependent on the amount of registered photons or ADUs as:

$$\sigma_{q,u,v} = kN^{-1/2}, \tag{6}$$

where k is the analyzer efficiency and $N = N_e + N_o$ is the total number of registered ADUs or counts. Thus, in order to achieve the precision at the level of 10^{-6} (part per million or ppm), 10^{12} ADUs must be collected. The early pixel saturation, a bottleneck for the CCD polarimeter when it is used for observation of the bright targets, normally is not an issue for the polarimeters equipped with a PMT detector. Moreover, the "instant" readout allows one to use PMT with the fast polarization modulator such as PEM or FLC. Not surprisingly, the PMT detectors have been used in the most precise polarimeters such as HIPPI (Bailey et al., 2015) and POLISH2 (Wiktorowicz and Nofi, 2015).

The major disadvantage of the PMT detectors is their relatively low quantum efficiency which is typically in the range 10–30%. The best in their class, super bialkali (SBA) and ultra bialkali (UBA) PMTs have QE $\simeq$ 40% with the peak near 400 nm. Thus, the polarimeters with PMT detectors, while being able to achieve an accuracy level of few ppm for bright stars, still cannot compete with the CCD polarimeters in the low flux domain. Because the PMT is a single-cell detector, it is suitable only for single target polarimetry of point-like objects. All existing PMT polarimeters utilize a diaphragm in the focal plane of the telescope, where the measured star is placed. The intensity and polarization of sky background are measured separately by either pointing the telescope away from the star to the clear area of the sky or with a separate sky registration channel.

2.4.3 Detectors for Optical Polarimetry: Avalanche Photo-Diodes

The *Avalanche Photo-Diode* or APD is the semiconductor analog to the PMT. In an APD, as with any other photodiode, incoming photons produce electron-hole pairs; however, the APD is operated with a large reverse *bias voltage* (up to 2 kV), which accelerates photoelectrons. Those electrons collide with atomic lattice, releasing additional electrons via secondary ionization. The secondary electrons are also accelerated, which results in an *avalanche* of charge carriers, hence the name.

Like the PMTs, APDs can work with high modulation frequencies (up to a few MHz) and can tolerate even higher fluxes, up to $\leq 10^9 e^-/\mathrm{s}$. They have a higher QE (up to 80% in the near IR) in comparison with the PMTs, but smaller or comparable QE in the blue wavelengths. The APDs have been used as detectors in PlanetPol (Hough et al., 2006), POLISH (Wiktorowicz and Matthews, 2008) and OPTIMA (Kanbach et al., 2008) polarimeters. Although the APD detectors may be better suitable for high-precision polarimetry of the bright targets in the near IR wavelengths, they do not offer significant advantage over the PMTs in the blue and visual spectral ranges. In comparison with the PMT (and CCD) detectors, the APDs have a higher dark current and are more noisy. Another disadvantage is the small effective photosensitive area, typically a few mm^2, which requires a very precise positioning of the telescope exit pupil on the detector surface.

It seems that APDs are becoming less popular detectors for high-precision optical polarimeters. The HIPPI (a successor to PlanePol) and POLISH2 (a successor to POLISH) are both employing PMTs.

3 Broadband, Imaging and Spectropolarimetry in the Optical Wavelengths

The various methods of measuring polarization in optical wavelengths can be divided in three distinct groups: *broadband polarimetry*, i.e., polarimetry of stellar-like objects with the use of broadband optical filters; *imaging polarimetry* of extended objects, like nebulae, usually made also with filters; and *spectropolarimetry*, i.e., measuring polarization over the regions of the optical spectrum with certain *spectral resolution*. Imaging polarimetry can be also done for the stellar-like targets. This method of observations has the advantage of simultaneous registration of sky background and comparison object which effectively shortens any exposure time.

3.1 Instruments for Broadband Optical Polarimetry

There are many instruments in this group utilizing different approaches and focused on achieving different goals. We give here a brief description of the most commonly used techniques and designs currently employed in optical broadband polarimetry.

3.1.1 Double-image CCD polarimeters

The layout of the most commonly used broadband optical CCD polarimeter is shown in Fig. 5. It consists of four parts: 1) detector (CCD camera); 2) filter wheel; 3) rotatable half wave (HWP) or quarter wave plate (QWP); and 4) double-beam polarization analyzer such as plane-parallel calcite (or Savart) plate or Wollaston prism. The rotation of the HWP (QWP) is normally done with the use of a high-precision *stepper motor*.

In order to measure *linear polarization*, a series of CCD images must be taken at the four positions of the HWP: 0°, 22.°5, 45° and 67.°5. Next step is to measure the intensities of the two orthogonally polarized stellar images I_e and I_o and compute their ratio $Q = I_e/I_o$. Then the normalized Stokes parameters q and u can be computed as:

$$Q_m = Q_0 + Q_{22.5} + Q_{45} + Q_{67.5}, \tag{7}$$

$$q = (Q_0 - Q_{45})/Q_m, \tag{8}$$

$$u = (Q_{22.5} - Q_{67.5})/Q_m. \tag{9}$$

Circular polarization can be measured with the QWP in the following way: two CCD images are taken at the positions of 45° and 135° (or −45° and 45°) and the degree of circular polarization $P_C = v$ is computed as:

$$Q_m = Q_{45} + Q_{135}, \tag{10}$$

$$v = 0.5\ (Q_{45} - Q_{135})/Q_m. \tag{11}$$

The setup shown on Fig. 5 can be used as a polarimetric "add-on" to a CCD photometer, a low resolution spectrograph or a multi-functional instrument. The rotated wave-plate and two-beam polarization analyzer can be moved into the optical path and removed when they are not necessary. This method of measurements, being simple, is probably the most efficient for the broad-band and low-resolution spectropolarimetry of faint point-like sources. Simultaneous registration of two polarized images (or spectra) helps to maximize efficiency and to avoid most of systematic errors. Currently it is used in several existing instruments, e. g., ALFOSC at the NOT, ORM (La Palma) and EFOSC and FORS2 at the ESO (Chile).

The layout shown above can be easily expanded and enhanced. For example, the DiPol-2 polarimeter shown in Fig. 6 does not have a filter wheel, but employs two dichroic beam-splitters installed after the polarization unit. The light beam is split into three passbands (B, V and R) registered with three CCD cameras simultaneously. Because DiPol-2 uses a plane-parallel calcite plate as a polarization analyzer, without having a focal plane mask, the o- and e-components of the sky overlap everywhere on the CCD image. Thus, the sky is not split into polarized components and sky polarization automatically cancels out when the total sky intensity $I_e + I_o$ is subtracted from the stellar images in data reductions (Piirola et al., 2014). DiPol-2 has been built in three copies and used for high-precision polarimetry of the low-mass X-rays binaries (Kosenkov et al., 2017; Veledina et al., 2019) (see Sect. 5.1), early-type binaries (Berdyugin et al., 2016, 2018) (see Sect. 5.2), novae (Harvey et al., 2018) and study of the interstellar polarization in the vicinity of the Sun (Frisch et al., 2015). DiPol-UF, a successor to DiPol-2, currently being built at the University of Turku, employs three ANDOR iXon Ultra 897 EMCCD cameras as detectors and has a retractable polarization unit which allows operation of the instrument also as a fast three-band photometer (simultaneous in BVR).

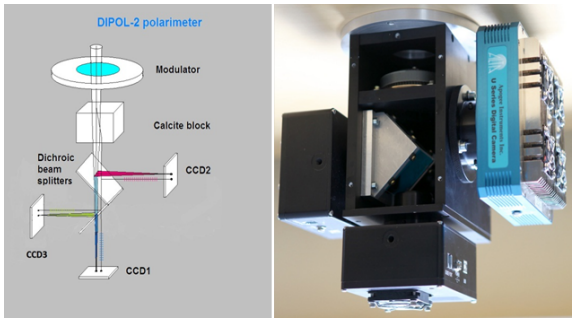

Fig. 6 Left: Schematic layout of the main components of the DiPol-2 polarimeter. Right: photo of DiPol-2 taken with the front cover removed. Polarization unit consisting of calcite, exchangeable retarder and stepper motor is installed in the upper section. Dichroic mirrors are installed in the lower section. Apogee Alta U47 CCD (B-band) is on the right side, two ST-402ME CCDs are on the left (R-band) and on the bottom (V-band).

3.1.2 High-Precision Double-Image Polarimeters with High-Frequency Modulators

There are several examples of currently existing instruments employing the techniques of fast modulation. One example is the UBVRI polarimeter *TurPol* (Piirola, 1973, 1988), the principal layout is shown in Fig. 7. In TurPol, the modulation of the incoming light, split by the calcite plate into two parallel beams, is done with a rotating mechanical chopper. The frequency of modulation is 25 Hz, which is enough to eliminate most of atmospheric effects. TurPol is equipped with a discretely rotated interchangeable $\lambda/2$ and $\lambda/4$ wave plates and is able to measure linear or circular polarization of the stellar-like objects with an accuracy up to a few times per 10^{-5} in the five UBVRI passbands simultaneously. The effect of sky polarization is canceled out due to the overlapping of the orthogonally polarized sky images in each of the two diaphragms. The total sky intensity $I_e + I_o$ is measured separately by pointing the telescope at the nearby clear area of the sky. TurPol has been made in several copies and still used for observations of polarization of various types of variable stars, studies of interstellar polarization and even for observations of exoplanets (Berdyugina et al., 2011). One of the main applications has been circular and linear polarimetry of magnetic Cataclysmic variables (e.g. Piirola et al., 1987, 1990, 1993, 2008), with orbital periods of a few hours and rapid variability on time scales from a fraction of a second to minutes. Simultaneous measurements in the different passbands are therefore essential.

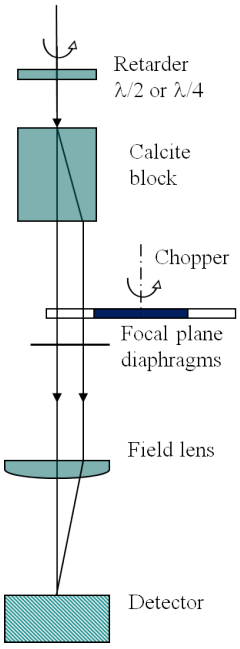

Fig. 7 The schematic layout of the TurPol polarimeter. The rotating chopper is installed after calcite block and in front of one of the selectable double diaphragms placed in the diaphragm wheel. After the double diaphragm, the field lens forms the exit pupil on the PMT detector. The registration of the intensities of e- and o-images of the star by the PMT is synchronized with the chopper rotation. In the real instrument, the light is split in five (U, B, V, R and I) beams by the four dichroic mirrors installed after the diaphragm section and registered simultaneously with the five PMTs.

Another example of a high-precision broadband instrument which was able to reach an accuracy in stellar optical polarimetry of the order of few ppm is the PlanetPol (Hough et al., 2006). This instrument uses PEM as a polarization modulator, three-wedged Wollaston prism as polarization analyzer and APD as detector. The working frequency of the PEM is $2f_0 = 40$ kHz and it operates as the $\lambda/2$ retarder. To measure both Stokes parameters of linear polarization, the whole instrument is rotated by 45°. Moreover, to minimize systematic errors, the lower section of the instrument with analyzer and detectors is rotated from −45° to +45°. The PlanetPol has two independent registration channels, one for the star (on axis) and one for the sky (off axis). The instrument has been designed to measure polarization in a wide wavelength range 470–910 nm, centered at the $\lambda = 690$ nm. The effective wavelength $\lambda_{\rm eff}$ is dependent on the spectral type and lies in the range of 735–805 nm.

PlanetPol has been mounted in the Cassegrain focus of the 4.2 m WHT telescope at the ORM (La Palma) and has measured polarization of a number of bright stars ($m_V \leq 5\overset{\rm m}{.}0$) with very impressive accuracy of few ppm (Bailey et al., 2010).

HIPPI, a successor to PlanetPol (Bailey et al., 2015), employs the FLC modulator, operated at the frequency of 500 Hz, and PMT detectors. Unlike PlanetPol, it is optimized for high-precision polarimetry in the blue wavelengths, in the spectral region ∼ 400–700 nm. Mounted on the 3.9 m Anglo-Australian Telescope, it was used for high-precision optical polarimetry of the nearby FGK dwarfs in the brightness range $m_V \simeq 0\overset{\rm m}{.}4 - 6\overset{\rm m}{.}0$. The achieved accuracy of polarization measurements (depending on brightness) is in the range of 1.5–10 ppm (Cotton et al., 2017).

POLISH2 polarimeter uses two PEM modulators operated at different frequencies to measure three Stokes parameters q, u and v in the UBV passbands (Wiktorowicz and Nofi, 2015). Reported accuracy of the instrument for observations of the bright "naked-eye" stars with the 3 m Shane telescope of the Lick Observatory is at the level of few ppm.

Such an impressive precision of polarimeters with fast modulators can be only achieved with careful calibration procedure which is necessary to take into account and minimize all sources of systematic errors. The accuracy at the level of $10^{-5} - 10^{-6}$ is only possible for bright stars and on telescopes with the aperture size ≥ 3 m. Thus, the primary goal of these instruments is limited to high-precision optical polarimetry of bright targets. An example of such application is a study of the interstellar polarization and direction of the local galactic magnetic field in the vicinity of the Sun (Frisch et al., 2015; Cotton et al., 2019). The intrinsically non-polarized stars of A, F, and G spectral types located at the distance <40 pc are bright, but show very low ($P \leq 0.01\%$ or $\leq 10^{-4}$) degree of interstellar polarization which can only be measured with the instruments providing precision at the level of 10^{-5} or better.

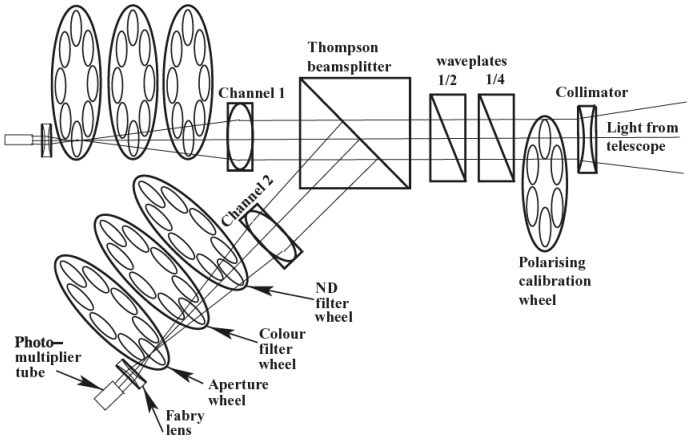

Fig. 8 The schematic layout of the HIPPO polarimeter. The HWP and QWP, placed in the collimated beam are contrarotated at frequency of 10 Hz modulating the polarization of the incoming light beam split by Thomson prism in e- and o-rays and registered separately by the two PMTs placed in Channels 1 and 2. Linear and circular only modes of polarimetry are possible and each channel can be used for independent measurements of three Stokes parameters with different filters. From Potter et al. (2010).

3.1.3 High-Speed Broadband Polarimeters for the Optical Wavelengths

Measuring polarization in the optical wavelengths with time resolution $\leq$ 1 s is a challenging task. An instrument capable to do this must be able to modulate the polarization of incoming light beam so as to have all Stokes parameters recorded in a short exposure time, and also to maintain a high light throughput. This is rather difficult to achieve in practice. The general approach for fast optical polarimetry is a continuous rotation of the wave-plate or polaroid with the frequency of few to 10 Hz.

HIPPO polarimeter, designed in the South African Astronomical Observatory (SAAO) is an example of an instrument built for high-speed photo-polarimetry of rapidly varying polarized astronomical sources, with particular interest in polarimetry of magnetic cataclysmic variables (mCVs). The layout of the instrument is shown in Fig. 8. HIPPO makes a single polarization measurement every 0.1 s (Potter et al., 2010). The acquired raw data, if necessary, can be binned to any integer multiple of 0.1 s.

Among the results obtained with HIPPO are the discovery of polarized QPOs in polar IGR J14536−5522 (Potter et al., 2010) and white dwarf pulsar AR Sco (Potter and Buckley, 2018). In both cases, the observations have been done with the 1.9 m telescope of the SAAO. The pulse periods, seen also in brightness variations are 5.2 and ∼2 min, respectively.

RINGO3[2] mounted on the robotic 2.0 m Liverpool Telescope at the ORM (La Palma) employs a rotated polaroid in front of the collimator, after which the light

[2] http://www.telescope.livjm.ac.uk/TelInst/RINGO3/

is split by two dichroic mirrors onto three Andor iXon 3 EMCCDs. After the year 2013, a Lyot depolarizer has been installed after the polaroid to get rid of the large instrumental polarization arising due to the dichroic mirrors. Initially the frequency of polaroid rotation was set to 1 Hz, which has allowed to measure the linear polarization two times per second. Currently the rotation frequency is set at ∼0.4 Hz.

The main shortcomings of the RINGO3, apart from rather large instrumental polarization, are significant overheads for initializing the instrument for the exposure and the loss of 50% of light intensity in the polaroid. Thus, the eight images acquired during one rotation cycle must be stacked over many cycles in order to achieve a reasonable S/N. The recommended minimum integration time is 20 s (Słowikowska et al., 2016).

The GASP polarimeter (Collins et al., 2013; Kyne et al., 2016) is a DOAP (division of amplitude polarimeter) which uses two EMCCDs with a timing resolution down to 500 microseconds. It measures both linear and circular polarization simultaneously with no moving parts.

We note that although the best high-speed polarimeters like HIPPO and GASP can sample the polarization with time resolution ≤ 0.1 s, the acquired Stokes parameters are usually binned over time intervals $\geq$ 10 s to achieve sufficient S/N. Thus, in the case of AR Sco, binning over 10 s has been made (Potter and Buckley, 2018). The binning interval for the polarization data collected for IGR J14536−5522 is not mentioned in the original paper, but it can be roughly estimated from the plots shown on Figs. 6 and 7 of the paper by Potter et al. (2010) as $\sim 30 - 60$ s. Both stars show rather strong (few percent of polarization) signal which is strictly periodic and this helps to reveal it from the raw data accumulated over the sufficiently long time span. Because the accuracy of polarimetry is critically dependent on the count rate, the small number of ADUs registered over short time interval is generally the problem in detecting weak short-term polarization signals.

It is worth to mention that for time resolution of $\geq$10 s the "traditional" CCD polarimeter with discretely rotated wave plate and fast readout CCD camera offers comparable, if not better performance. The single turn of the wave plate is done by stepper motor in 0.2–0.3 s. Thus, the time lost in wave plate rotation can be $\leq$ 0.5 s and $\leq$ 1.0 s for one cycle of circular and linear polarization measurements, respectively. Stepper motors are compact, precise and provide reliable long-term operation. Moreover, modern EMCCD cameras offer frame rates of few tens per second and are able to "stack" images, thus allowing to shorten the sampling time interval considerably.

3.2 Instruments for Optical Imaging Polarimetry

3.2.1 Optical Imaging Polarimetry with Polaroids

The simplest way to measure polarization of extended objects is to take a series of CCD images with a polaroid filter. Normally, four images are taken at $0°, 45°, 90°$ and $145°$ orientations of the polaroid. Because the images for the polarimetry cycle are not taken simultaneously, any variations in the atmospheric transparency will give spurious polarization signal. Hence, this method of measurement can be applied only in strictly photometric nights. The calibration flat field must be obviously taken separately for each orientation of the polaroid. This method of imaging polarimetry has been used at the NOT (La Palma) with the ALFOSC (see, for example, Piirola et al., 1992; Harjunpää et al., 1999).

3.2.2 Optical Imaging Polarimetry with a Double-Beam Analyzer and Stripe Mask

The problems with atmospheric transparency variations and light losses in the polaroid can be solved with the use of a double-beam analyzer and a *stripe mask*. The FOcal Reducer and low dispersion Spectrograph (FORS2) mounted on the Cassegrain focus of the 8.2 m UT1 telescope at the ESO (Chile) is equipped with a mask that can be inserted in the focal plane before the collimator, to avoid overlapping of the two orthogonally polarized beams produced by the Wollaston prism on the CCD. With this mask, a full scan of the imaging field is achieved by taking two series of frames displaced by $22''$.[3] This allows one to do imaging polarimetry of extended objects and crowded stellar fields.

Unfortunately, FORS has a strong field dependent off-axis instrumental linear polarization which seriously compromises the performance of the instrument for multi-target or extended object polarimetry.[4] Hence, this instrument is mostly used for broadband and spectropolarimetry of single targets in the center of the field of view.

3.2.3 Optical Imaging Polarimetry with Fast-Frequency Modulators and Fast-Readout CCDs

The idea of using fast-readout EMCCD cameras in combination with the FLC modulators for optical imaging polarimetry is attractive. An example of this approach is the GREGOR Planet Polarimeter (GPP, Gisler et al., 2016). This design eliminates the necessity to use the stripe mask and allows recording of the two orthogonally

[3] http://www.eso.org/sci/facilities/paranal/instruments/fors/doc/VLT-MAN-ESO-13100-1543_v83.pdf

[4] http://www.eso/org/sci/facilities/paranal/instruments/fors/inst/pola.html

polarized images simultaneously and synchronously with the fast modulation and two EMCCD cameras.

The layout of GPP is shown in Fig. 9. GREGOR is a 1.5 m solar telescope located at the Observatorio del Teide, Tenerife. This telescope, which is a double Gregory-type design, can be also employed for night-time observations. The polarimeter is located on the stationary optical bench after the 50/50 cube beam splitter which reflects part of the light to the wave front sensor. The transmitted light is used by the polarimeter. The camera lens (see Fig. 10) images the focal plane to the CCD cameras with a resolution of 0.″086/pixel. The polarization unit consists of modulator and analyzer. The modulator unit has two FLCs and two wave-plates which allows to measure all Stokes parameters. A polarizing beam-splitter cube (PBC) is used as the analyzer. Two interchangeable modulators optimized for the the blue-visible and visible - read spectral regions can be used. The modulation frequency is determined by the ANDOR iXon Ultra 897 camera frame rates. For the full frame images it is 14 Hz. For the sub-frame imaging mode, e.g. used for polarimetry of Uranus and Neptune, with the frame size of 128×128 pixels, the modulation frequency is 150 Hz (see Gisler et al., 2016).

The polarimeter can measure all Stokes parameters either with a single or two CCD cameras at the same time. Due to multiple reflections in telescope mirrors and alt-azimuth mount, the telescope instrumental polarization is high and variable. To account for it, GREGOR has a special polarimetric calibrating unit installed in the telescope before the first diagonal mirror. The calibration procedure consists of taking calibration measurements at the same position as the object observed at the sky. Currently only relative calibration of polarization within the image is possible, but the artificial unpolarized flat field light source will be implemented in the future. This should allow an absolute calibration of polarization image.

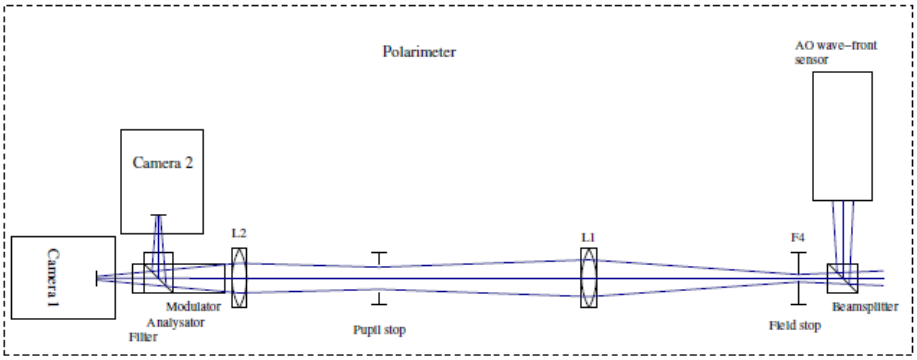

Fig. 9 The schematic layout of the GPP imaging polarimeter. The field stop (iris diaphragm) and pupil stop are used to block the unwanted part of the light. L1 and L2 are collimating and imaging lenses. After L2 the modulator is installed, followed by PBC unit. The filters can be inserted either in front of modulator or after analyzer. From Gisler et al. (2016).

3.3 Instruments for Optical Spectropolarimetry

In many cases, spectropolarimetry in the optical wavelengths can be done by adding the polarization modulator and analyzer to the optical path of the spectrograph. This method is well suitable for low and intermediate resolution spectropolarimetry and has been implemented in many existing instruments (see Section 3.1.1). The processes of data acquisition and data reduction do not differ much from those applied for traditional spectroscopy where only $I(\lambda)$ is registered (Section 2.4.1.)

3.3.1 Instruments for Low and Mid-Resolution Optical Spectropolarimetry

One example of a multi-functional instrument with spectropolarimetry observation mode implemented is FORS2. The polarization unit consists of a discretely rotated wave plate (HWP or QWP), placed after the collimator into the parallel beam with the dedicated swing arm, and Wollaston prism, mounted in the uppermost filter wheel. With the inserted polarization optics, spectropolarimetry can be done with most of the available grisms, with the spectral resolution $\lambda/\Delta\lambda$ from 450 to 2500. FORS2 employs superachromatic wave plate mosaics (3×3) and can be used for single and multi-object spectropolarimetry in the spectral range 330–1100 nm.

Spectropolarimetry can be done with the two CCD mosaics, either with the two $2k \times 4k$ MIT CCDs optimized for the red part of spectrum or with two $2k \times 4k$ E2V CCDs particularly sensitive in the blue range. Because FORS2 is mounted in the Cassegrain focus, it benefits from the very low telescope polarization (in the center of the field of view) and thus is well suitable for the absolute linear and circular spectropolarimetry of faint objects, being one of the best instruments in this class. FORS1 (a retired twin of FORS2) has been extensively used for the study of stellar magnetic fields with spectropolarimetry (see, for example, Bagnulo et al., 2002, 2006; Vornanen et al., 2010).

Spectropolarimetry with ALFOSC on the 2.52 m Nordic Optical Telescope (NOT) at the ORM (La Palma) is done with the HWP or QWP plates mounted in the converging beam (before the focal plane) and calcite beam-splitter mounted in the aperture wheel. The spectral resolution in the wavelength range 320–1100 nm can be selected from 210 (with the low-res, wide spectral range grism) up to 10000 (high-res grism, centered at the Hα).

3.3.2 Instruments for High-Resolution Optical Spectropolarimetry

The most important application of high-resolution spectropolarimetry is for study of magnetic fields in solar-type stars. Spectral resolution higher than ~ 50000 normally requires an échelle spectrograph.

Good example of a polarimeter implemented to a high-resolution échelle spectrograph is PEPSI (Potsdam Echelle Polarimetric and Spectroscopic Instrument) built for the 8.2 m Large Binocular Telescope (LBT). The design allows to measure all

four Stokes parameters (I, Q, U and V) with two identical independent polarimeters at the spectral resolution of 130000 (Strassmeier et al., 2015). These polarimeters are installed at the straight-through f/15 Gregorian foci of the LBT. The entire PEPSI light feed is split into the *integral light* part with the permanent focus and *polarimetric-light* part which is available after dismounting other instruments (see Strassmeier et al., 2015, for further details).

The polarimeter units are of double-beam type with a Foster prism beam-splitter used as the polarization analyzer. For measuring linear polarization the analyzer unit is rotated. For measuring circular polarization, a superachromatic QWP is inserted into the light beam. The principal layout of the instrument is shown in Fig. 10. Detailed description of the instrument can be also found in Ilyin et al. (2011). Spectropolarimetry with high-resolution spectrographs which always employ a significant number of reflecting optical elements, échelle grating, multiple mirrors, fibers etc., requires careful calibration of the instrumental polarization (e.g. Ilyin, 2012). The calibration process involves modeling the transformation of the Stokes parameters in the telescope and polarimeter optics with the Mueller matrices. The precise calibration is normally done with the use of polarized calibration light sources inserted into the optical path.

4 Calibration Techniques for Optical Polarimetry

The advantage of polarimetry over photometry is that the measurement is based on the *relative* intensity of two perpendicularly polarized components of light, rather than the total intensity measured in photometry. That helps in eliminating effects from variable atmospheric transmission and the throughput of the instrument. However,

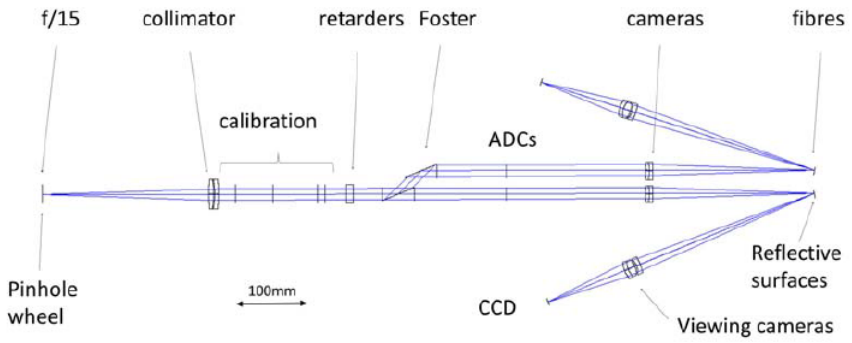

Fig. 10 Optical design of the PEPSI spectropolarimeter. The light enters from the left and exit into the fibers to the spectrograph section on right. The fibers are positioned on the central pinholes in the reflective surfaces. The individual optical components are marked. ADCs are the atmospheric dispersion correctors. The calibration components and QWP unit are retractable. From Strassmeier et al. (2015).

on the counterside is the very minute amount of polarization seen in astronomical objects, rarely exceeding a few percent and in the most demanding applications detection sensitivity at the ppm level (10^{-6}) is required.

4.1 Calibration of Linear Polarization

In case of linear polarization measurements, the calibration has to be carried out for:

1. Polarization scale,
2. Zero-point of polarization angle,
3. Instrumental polarization produced by the polarimeter,
4. Polarization produced by the telescope optics.

A straightforward way of polarization scale calibration (1) is to insert a high quality polarizer, e.g. a Glan prism with a nearly 100% efficiency, in front of the polarimeter. The scale calibration is particularly important for the high frequency modulators, where the efficiency can be as low as $\sim$ 70% and strongly dependent on the wavelength, as the modulators are not achromatic. Double image polarizers, like calcite plate and Wollaston prism, have practically 100% efficiency. If the whole polarimeter is rotated at 45° steps, virtually no polarization scale calibration is then needed. Superachromatic retarder plates with excellent performance in the 310–1100 nm range are available, but scale correction factors up to 1.02–1.03 may be encountered also with these devices. In practice, if no scale calibration optical component is available, one has to trust on published high polarization standards to correct for the polarimeter efficiency factor.

For the angle calibration (2) one may use a high quality polarizer oriented accurately in a known, e.g. equatorial, frame of references. The double image polarizers, calcite and Wollaston prism, are particularly advantageous in this regard, because they provide images with know polarization orientation, readily fixed in the celestial coordinate system by the line connecting the two images. For that reason a rotatable (45° steps) double image polarimeter is an ideal instrument for establishing high polarization standards, both for the scale and the angle calibration. Superachromatic retarder plates are less favorable for the highest precision angle calibration, because their optical axis typically varies in a complex way by several degrees over the wavelength regions applied. Therefore, it is also crucial not to use too broad passbands ($<$ 100 nm) if the angle calibration is critical. Differences in spectral energy distribution could easily introduce noticeable shifts in the effective wavelength and thereby errors in the corrections applied.

The best way of eliminating the instrumental polarization (3) produced by the polarimeter ($q_{\rm in}$, $u_{\rm in}$) is to rotate the whole instrument through 360° by 45° steps for one complete measurement. Typically, rotation effects (optics misalignments etc.) create a sinusoidal spurious modulation, but since the stellar polarization gives a *double* sinusoid, the instrumental effects are largely canceled in the reductions. Rotating the whole polarimeter, however, is often undesirable and a rotated retarder

is used instead. Similarly, the half-wave plate must be rotated full 360° cycles (22.°5 steps) to get the best accuracy and avoid effects from e.g. dust particles on the retarder, non-parallelism of rotating components, etc.

Eliminating the spurious polarization produced by the telescope optics (4) is perhaps the most difficult part to establish without leaving residual systematic errors, if the highest precision (a few ppm level) is required. Such a source like an "unpolarized star" probably does not exist. Stellar chromospheric activity may lead to detectable, and variable, intrinsic polarization even for "normal" A-G main sequence stars. For a reliable determination it is necessary to observe a sample of (5 – 20) nearby stars ($d < 25$ pc, if possible) and obtain the normalized Stokes parameters of the telescope polarization, ($q_{\rm tel}$, $u_{\rm tel}$) as the average of the (q, u) of the observed sample of stars. In this way also small effects of interstellar polarization present in each of the observed stars will tend to cancel out.

Alt-az telescopes provide an additional way of determining ($q_{\rm tel}$, $u_{\rm tel}$). Because the field angle of the telescope optics continuously changes on the sky, this gives polarization modulation: a double cosine curve over one full rotation. Fitting curve to this modulation yields the amplitude and angle of the telescope polarization in the telescope optics coordinate system. These can then be rotated to the equatorial frame of references for the moment of the observation and subtracted from the stellar observation.

There are numerous ways, in addition to curve fitting, to determine the ($q_{\rm tel}$, $u_{\rm tel}$) for an alt-az telescope. During observations the polarimeter is rotated with respect to the telescope to keep it in the equatorial system. The observed (q, u) of zero-polarization standard stars can be rotationally transformed to the telescope optics system. After the transformation, the ($q_{\rm tel}$, $u_{\rm tel}$) values are obtained by averaging the (q, u) values of the standard stars in the telescope frame of references. Also iterative methods can be applied to get both ($q_{\rm in}$, $u_{\rm in}$) and ($q_{\rm tel}$, $u_{\rm tel}$) from the same sample of calibration measurements.

Equatorial mounted telescope is convenient in the sense that the telescope polarization does not rotate on the sky. It only gives a constant shift in (q, u). This is particularly important for searching small short-term periodic variations in binary and multiple stars, exoplanet systems, etc. Any residual telescope polarization does not change the shape of the observed phase-locked patterns of the normalized Stokes parameters (q, u). The curves are only shifted by the amount of uncorrected ($q_{\rm tel}$, $u_{\rm tel}$), similarly to the effect of interstellar polarization.

4.2 Calibration of Circular Polarization

The telescope *circular* polarization ($v_{\rm tel}$) is of an order of magnitude smaller than linear and, therefore, can be ignored in many applications. However, the effect of *cross-talk*, i. e. the transformation of high linear polarization into circular which may occur in the telescope or polarimeter optics, must be carefully investigated and taken into account. The sign of the circular polarization can be calibrated with the

observations of the magnetic white dwarfs with the strong and non-variable circular polarization, e.g. Grw+70 8247 which has $P_C \simeq -4.0\%$ in the B-band.

4.3 Calibration of the CCD Polarimetry: Flatfielding

Standard CCD reductions, bias, dark, and flat field calibrations are obviously applied in the first part of the reduction pipeline scripts. Our experience with double image polarimeters having a rotatable superachromatic retarder (DiPol-1 and DiPol-2), and spectropolarimeters (ALFOSC at the NOT, EFOSC and FORS at the ESO), is that it is best not to apply different flat fields for each of the different position angle of the retarder, but use the same flat field for all (16) retarder positions. Individual flats fail to improve the precision, on the contrary. Common flat field is enough to suppress pixel-to-pixel variations in the CCD sensitivity. Measuring sequences consisting of cycles made over full rotation of the retarder make the polarimeter rather insensitive to flat field imperfections.

ESO staff recommends to take sky flats for calibration of polarimetry images acquired with the FORS with the *polarization optics removed*. The reason for this is that the sky flat itself can be polarized. To avoid possible errors, it is advisable always to take sky flats in the direction of sky opposite to the rising or setting Sun.

For the highest S/N measurements it is advantageous to strongly defocus images to spread light over a very large number of pixels (Piirola et al., 2014). In this way we can expose up to 10^8 electrons in one stellar image without saturating the CCD pixels. Even if there are minor shifts in the position of the two perpendicularly polarized images of the target, vast majority of the pixels remain the same over the full measurement cycle (16 exposures). Minor imperfections in the flat field are eliminated in the reductions, since the ratio of the o- and e- beam transmission and efficiency, if constant, is automatically cancelled in the reduction algorithm. This provides inherently very stable instrument and detection sensitivity better than 10^{-5} (< 10 ppm) in $\sim$1 hour for sufficiently bright stars. In fact, e.g. DiPol-2 polarimeter is photon-noise limited down to these very low polarization signal levels.

5 High-precision CCD polarimetry of binary stellar systems

One important application of optical polarimetry is to study interacting binary stars. The interaction, which involves transfer of matter from one component to another, very often gives rise to variable linear polarization due to the light scattering on the circumstellar material such as gaseous streams, disks, jets and non-spherical envelopes. In binary systems with accreting black hole component, linear polarization may also arise due to synchrotron radiation emitted in the jet. Thus, polarimetry of these objects can provide useful information on their physical properties. Below

we provide examples of high-precision measurements of polarization in black hole X-ray binaries and in early type binaries, made with the DiPol-2 instrument.

5.1 Polarimetry of black hole X-ray binaries

The low-mass black hole X-ray binary V404 Cyg went into outburst in 2015 after being 26 years in quiescence. In the peak of the outburst, the object showed very erratic behaviour with flares reaching a few tens of Crab in the hard X-ray domain, which for the known distance of 2.4 kpc corresponds to the Eddington luminosity for a 10 $M_\odot$ black hole (Rodriguez et al., 2015; Motta et al., 2017). The object also showed strong variability in the optical (see Kimura et al., 2016, and also lower left panel of Fig. 11). In order to understand the nature of the optical emission we performed simultaneous three-colour (BVR) polarimetric observations during and after the outburst (see Kosenkov et al., 2017, for details). We detected small but statistically

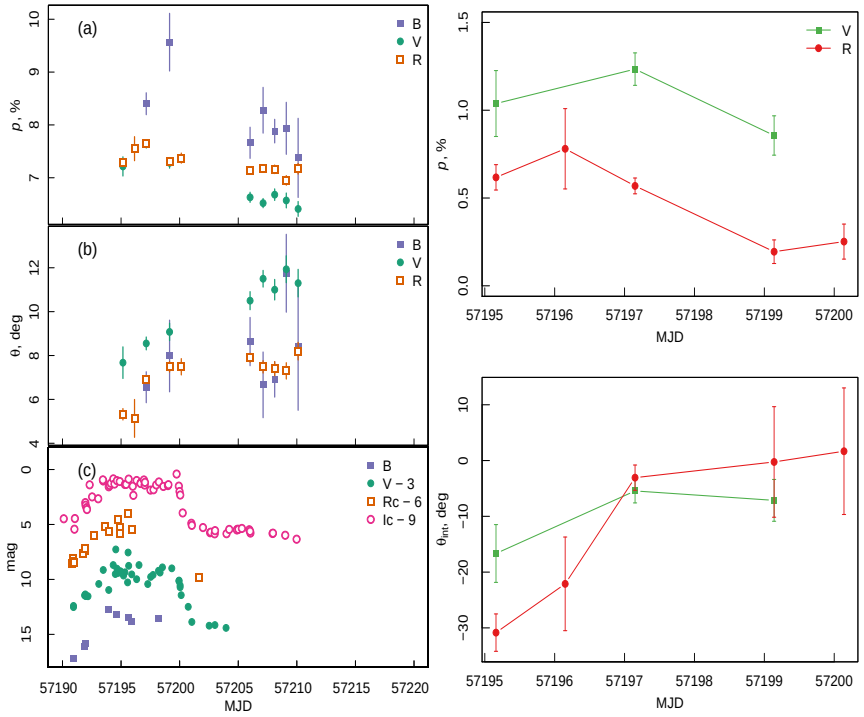

Fig. 11 The 2015 June-July outburst of the black hole X-ray binary V404 Cyg. *Left*: panels (a) and (b) show the observed linear PD (p) and PA (θ) in three bands; and panel (c) gives the optical light curve. *Right*: variations of the intrinsic linear PD (p) and PA (θ) in the V and R bands over the outburst. From Kosenkov et al. (2017).

significant change of the linear PD by ∼1% between the outburst and the quiescence (see left panels of Fig. 11). We also found that the polarization of V404 Cyg in the quiescent state agrees well with that of the visually close (1.″4) companion, as well as those of the surrounding field stars, indicating that it is predominantly of interstellar origin. From the observed variable polarization during the outburst we showed that the intrinsic polarization component peaks in the V band with $PD_V = 1.1 \pm 0.1\%$, and in the R band it is factor of two smaller $PD_R = 0.46 \pm 0.04\%$, while the polarization PA $(\theta) = -7^\circ \pm 2^\circ$ is similar in all three passbands. The observed wavelength dependence of the intrinsic polarization does not support non-thermal synchrotron emission from a jet as a plausible mechanism, but is in better agreement with the combined effect of electron (Thomson) scattering and absorption in a flattened plasma envelope or outflow surrounding the illuminating source. Interestingly, we also found that the PA of the intrinsic polarization is nearly parallel to the jet direction (i.e. perpendicular to the accretion disc plane) as determined by the VLBI observations.

Another black hole X-ray transient MAXI J1820+070 went into a spectacular outburst in March 2018. In the X-rays the source flux exceeded 3 Crabs and in the optical reached magnitude m_V =12–13. This unusually bright event allowed detailed investigation of multiwavelength spectral and timing properties and the source was monitored from radio to the γ-rays. Fast variability and powerful flares in the optical and infrared as well as optical and X-ray quasi-periodic oscillations were detected in the source. To disentangle sources of optical emission we performed BVR polarization measurements during March-April 2018 (see Veledina et al., 2019, for details). We detected small, ∼0.7–0.9%, but statistically significant linear polarization at PA of about 50° in all filters. We also detected a significant change in the PD after 2018 April 14 (see right panels in Fig. 12). The change is of the order of 0.1% and is most pronounced in the R band. By analyzing a set of nearby field stars, we were able to determine the contribution of the interstellar polarization. This allowed us to obtain the intrinsic polarization of MAXI J1820+070 at the level of 0.3–0.5%, depending on the filter (see middle right panel in Fig. 12). The change of the source Stokes vector occurred simultaneously with the drop of the observed V magnitude and a slow softening of the X-ray spectrum, which we interpreted as a signature of an evolution towards the soft state. The increased polarization may be a result of the decreasing contribution of the non-polarized component which we can associate with the hot flow or a jet. Its low polarization likely results from the tangled geometry of the magnetic field or from the Faraday rotation in the dense, ionized and magnetized medium close to the black hole. We argued that the polarized optical emission is produced by the irradiated disc or scattering of its radiation in the optically thin outflow.

5.2 Polarimetry of early type binaries

In massive early-type binaries and various interacting systems (e.g. Algol-type), orbitally phase-locked linear polarization may arise due to electron (Thomson) scat-

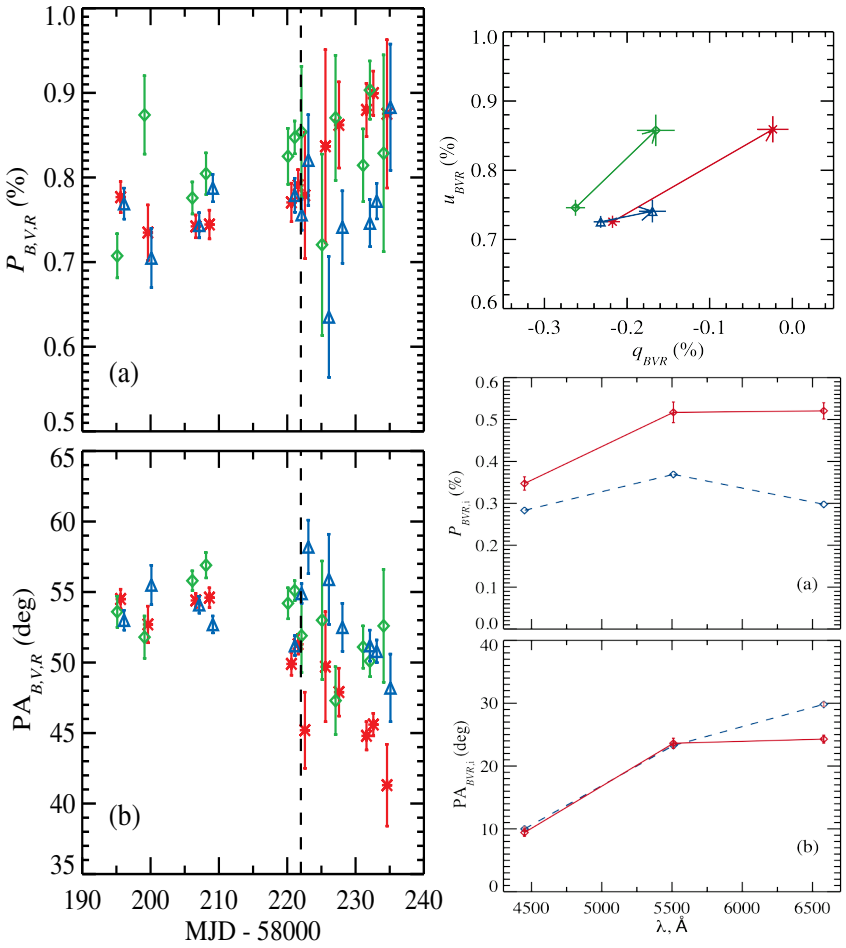

Fig. 12 Polarization properties of black hole X-ray binary MAXI J1820+070. Left panels: Evolution of (a) PD (P) and (b) PA in different filters: B (blue triangles), V (green diamonds) and R (red crosses). The vertical dashed line marks MJD 58222 (2018 April 14), after which we detected a significant increase of polarization. Right upper panel: Observed polarization in three filters (B - blue triangles, V - green diamonds and R - red crosses) in the Stokes (u, q)-parameter plane before (lower left symbols) and after MJD 58222 (upper right symbols). Arrows show the direction of polarization change. Right two lower panels: Wavelength dependence of the *intrinsic* (a) PD (P) and (b) PA. Weighted averages are shown with the blue dashed and red solid lines for observations before and after MJD 58222, respectively. Adapted from Veledina et al. (2019).

tering. A detailed analysis of the polarization variability yields independent estimates of the orbital orientation Ω and inclination i (e.g. Brown et al., 1978). The amplitude of the variability depends on the amount of the light-scattering material and usually is $\leq 10^{-3}$. In order to detect this variability, a high precision, at the level of 10^{-4} or

better, is necessary. Examples of applications of CCD polarimetry on such binary systems are given in Figs. 13 and 14.

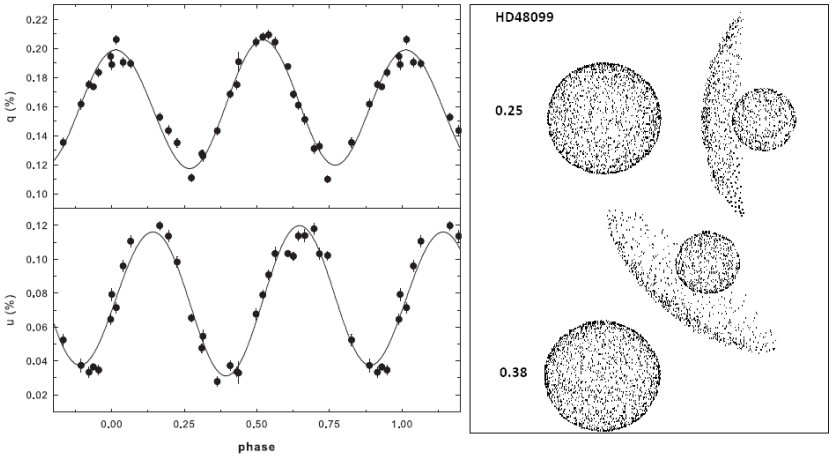

Fig. 13 Polarization variability in HD48099. *Left*: Observed Stokes parameters q and u in the B-band, plotted over the phase of the orbital period. The vertical bars show 2σ errors. *Right*: The scattering model showing O-type components and the light scattering cloud produced by colliding stellar winds at the different phases of orbital period. Adapted from Berdyugin et al. (2016).

HD48099 (Fig. 13) is a massive, detached early-type binary consisting of O5.5 V and O9 V stars. The orbital period is ∼3.08 days and there is evidence of colliding stellar winds the system (e.g. Mahy et al., 2010). This binary is non-eclipsing, and an independent estimate of the orbital inclination, provided by polarimetry, is important for constraining the component masses.

In Fig. 14 we show our results for λ Tau, a "classic" Algol-type triple system with the inner binary consisting of a more evolved and less massive mid-A type secondary filling its Roche lobe and a more massive B3 V primary star. The orbital period of the inner pair is ∼3.95 days. The unseen tertiary star (most probably a K dwarf) orbits around the inner binary with the period of ∼33 days (e.g. Fekel and Tomkin, 1982).

In both cases, small-amplitude variations of polarization (∼0.1% for HD48099 and ∼0.05% for λ Tau) have been revealed with DiPol-2 polarimetry. Modelling the polarization data yielded the determination of the orbital parameters and the location of light scattering material (Berdyugin et al., 2016, 2018).

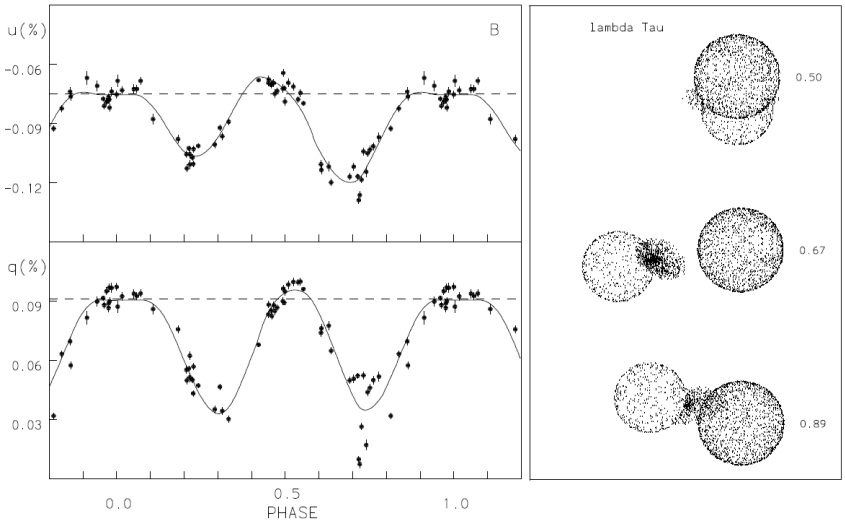

Fig. 14 Polarization variability in λ Tauri. *Left*: Observed Stokes parameters q and u in the B-band plotted over the phase of the orbital period. The vertical bars show 2σ errors. *Right*: The scattering model showing primary and secondary components with the light scattering cloud between them at the different phases of orbital period. Adapted from Berdyugin et al. (2018).

6 Summary

In this chapter we reviewed the methods, instruments and calibration techniques used in modern astronomical optical polarimetry. We described the properties of various polarization devices and detectors used for optical broadband, imaging and spectropolarimetry, and discussed their advantages and disadvantages. We stressed the necessity to properly calibrate the raw polarization data, and discussed the methods of the determination of instrumental polarization and its subtraction. Finally, we presented a few examples of high-precision measurements of optical polarization in two black hole X-ray binaries and massive binary stars made with our DiPol-2 polarimeter, which allowed us to obtain interesting constraints on the origin of optical emission in black hole X-ray binaries and on the orbital parameters of massive stellar binaries.

Acknowledgements

We acknowledge support from the ERC Advanced Grant HotMol ERC-2011-AdG-291659 (AVB). The DiPol-2 was built in cooperation between the University of Turku, Finland, and the Kiepenheuer Institut für Sonnenphysik, Germany, with support from the Leibniz Association grant SAW-2011-KIS-7.

References

Bagnulo S, Szeifert T, Wade GA, Landstreet JD, Mathys G (2002) Measuring magnetic fields of early-type stars with FORS1 at the VLT. A&A 389:191–201, DOI 10.1051/0004-6361:20020606

Bagnulo S, Landstreet JD, Mason E, Andretta V, Silaj J, Wade GA (2006) Searching for links between magnetic fields and stellar evolution. I. A survey of magnetic fields in open cluster A- and B-type stars with FORS1. A&A 450:777–791, DOI 10.1051/0004-6361:20054223, astro-ph/0601516

Bailey J, Lucas PW, Hough JH (2010) The linear polarization of nearby bright stars measured at the parts per million level. MNRAS 405:2570–2578, DOI 10.1111/j.1365-2966.2010.16634.x, 1003.1753

Bailey J, Kedziora-Chudczer L, Cotton DV, Bott K, Hough JH, Lucas PW (2015) A high-sensitivity polarimeter using a ferro-electric liquid crystal modulator. MNRAS 449:3064–3073, DOI 10.1093/mnras/stv519, 1503.02236

Berdyugin A, Piirola V, Sadegi S, Tsygankov S, Sakanoi T, Kagitani M, Yoneda M, Okano S, Poutanen J (2016) High-precision broad-band linear polarimetry of early-type binaries. I. Discovery of variable, phase-locked polarization in HD 48099. A&A 591:A92, DOI 10.1051/0004-6361/201528020, 1606.00198

Berdyugin A, Piirola V, Sakanoi T, Kagitani M, Yoneda M (2018) High-precision broad-band linear polarimetry of early-type binaries. II. Variable, phase-locked polarization in triple Algol-type system λ Tauri. A&A 611:A69, DOI 10.1051/0004-6361/201732163

Berdyugina SV, Berdyugin AV, Fluri DM, Piirola V (2011) Polarized Reflected Light from the Exoplanet HD189733b: First Multicolor Observations and Confirmation of Detection. ApJ 728:L6, DOI 10.1088/2041-8205/728/1/L6, 1101.0059

Brown JC, McLean IS, Emslie AG (1978) Polarisation by Thomson scattering in optically thin stellar envelopes. II - Binary and multiple star envelopes and the determination of binary inclinations. A&A 68:415–427

Collins P, Kyne G, Lara D, Redfern M, Shearer A, Sheehan B (2013) The Galway astronomical Stokes polarimeter: an all-Stokes optical polarimeter with ultra-high time resolution. Experimental Astronomy 36:479–503, DOI 10.1007/s10686-013-9342-5, 1305.6825

Cotton DV, Marshall JP, Bailey J, Kedziora-Chudczer L, Bott K, Marsden SC, Carter BD (2017) The intrinsic and interstellar broad-band linear polarization of nearby FGK dwarfs. MNRAS 467:873–897, DOI 10.1093/mnras/stx068, 1701.02890

Cotton DV, Marshall JP, Frisch PC, Kedziora-Chudzer L, Bailey J, Bott K, Wright DJ, Wyatt MC, Kennedy GM (2019) The wavelength dependence of interstellar polarization in the Local Hot Bubble. MNRAS 483:3636–3646, DOI 10.1093/mnras/sty3318, 1812.00294

Fekel FC Jr, Tomkin J (1982) Secondaries of eclipsing binaries. IV - The triple system Lambda Tauri. ApJ 263:289–301, DOI 10.1086/160503

Finger G, Baker I, Alvarez D, Ives D, Mehrgan L, Meyer M, Stegmeier J, Weller HJ (2014) SAPHIRA detector for infrared wavefront sensing. In: Adaptive Optics Systems IV, Proc. SPIE , vol 9148, p 914817, DOI 10.1117/12.2057078

Frisch PC, Berdyugin A, Piirola V, Magalhaes AM, Seriacopi DB, Wiktorowicz SJ, Andersson BG, Funsten HO, McComas DJ, Schwadron NA, Slavin JD, Hanson AJ, Fu CW (2015) Charting the Interstellar Magnetic Field causing the Interstellar Boundary Explorer (IBEX) Ribbon of Energetic Neutral Atoms. ApJ 814:112, DOI 10.1088/0004-637X/814/2/112, 1510.04679

Gisler D, Berkefeld T, Berdyugina S (2016) Planet imaging polarimetry with the solar telescope GREGOR. In: Ground-based and Airborne Telescopes VI, Proc. SPIE , vol 9906, p 99065E, DOI 10.1117/12.2233461

Harjunpää P, Kaas AA, Carlqvist P, Gahm GF (1999) Linear polarization and molecular filamentary clouds. A&A 349:912–926

Harvey EJ, Redman MP, Darnley MJ, Williams SC, Berdyugin A, Piirola VE, Fitzgerald KP, O'Connor EGP (2018) Polarimetry and spectroscopy of the "oxygen flaring" DQ Herculis-like nova: V5668 Sagittarii (2015). A&A 611:A3, DOI 10.1051/0004-6361/201731741, 1802.00224

Hough JH, Lucas PW, Bailey JA, Tamura M, Hirst E, Harrison D, Bartholomew-Biggs M (2006) PlanetPol: A Very High Sensitivity Polarimeter. PASP 118:1302–1318, DOI 10.1086/507955

Ilyin I (2012) Second-order error propagation in the Mueller matrix of a spectropolarimeter. Astronomische Nachrichten 333:213, DOI 10.1002/asna.201211652

Ilyin I, Strassmeier KG, Woche M, Dionies F, Di Varano I (2011) On the design of the PEPSI spectropolarimeter for the LBT. Astronomische Nachrichten 332:753, DOI 10.1002/asna.201111600

Kanbach G, Stefanescu A, Duscha S, Mühlegger M, Schrey F, Steinle H, Slowikowska A, Spruit H (2008) OPTIMA: A High Time Resolution Optical Photo-Polarimeter. In: Phelan D, Ryan O, Shearer A (eds) High Time Resolution Astrophysics, Astrophysics and Space Science Library, vol 351, p 153

Kemp JC (1981) Photoelastic-modulator polarimeters in astronomy. In: Trapani G (ed) Polarizers and applications, Proc. SPIE , vol 307, pp 83–88

Kimura M, Isogai K, Kato T, Ueda Y, Nakahira S, Shidatsu M, Enoto T, Hori T, Nogami D, Littlefield C, Ishioka R, Chen YT, King SK, Wen CY, Wang SY, Lehner MJ, Schwamb ME, Wang JH, Zhang ZW, Alcock C, Axelrod T, Bianco FB, Byun YI, Chen WP, Cook KH, Kim DW, Lee T, Marshall SL, Pavlenko EP, Antonyuk OI, Antonyuk KA, Pit NV, Sosnovskij AA, Babina JV, Baklanov AV, Pozanenko AS, Mazaeva ED, Schmalz SE, Reva IV, Belan SP, Inasaridze RY, Tungalag N, Volnova AA, Molotov IE, Miguel ED, Kasai K, Stein WL, Dubovsky PA, Kiyota S, Miller I, Richmond M, Goff W, Andreev MV, Takahashi H, Kojiguchi N, Sugiura Y, Takeda N, Yamada E, Matsumoto K, James N, Pickard RD, Tordai T, Maeda Y, Ruiz J, Miyashita A, Cook LM, Imada A, Uemura M (2016) Repetitive patterns in rapid optical variations in the nearby black-hole binary V404 Cygni. Nature 529:54–58, DOI 10.1038/nature16452, 1607.06195

Kosenkov IA, Berdyugin AV, Piirola V, Tsygankov SS, Pallé E, Miles-Páez PA, Poutanen J (2017) High-precision optical polarimetry of the accreting black hole V404 Cyg during the 2015 June outburst. MNRAS 468:4362–4373, DOI 10.1093/mnras/stx779, 1702.02008

Kyne G, Lara D, Hallinan G, Redfern M, Shearer A (2016) An investigation of the Eigenvalue Calibration Method (ECM) using GASP for non-imaging and imaging detectors. Experimental Astronomy 41:43–66, DOI 10.1007/s10686-015-9464-z, 1509.05270

Mahy L, Rauw G, Martins F, Nazé Y, Gosset E, De Becker M, Sana H, Eenens P (2010) A New Investigation of the Binary HD 48099. ApJ 708:1537–1544, DOI 10.1088/0004-637X/708/2/1537, 0912.0605

Motta SE, Kajava JJE, Sánchez-Fernández C, Beardmore AP, Sanna A, Page KL, Fender R, Altamirano D, Charles P, Giustini M, Knigge C, Kuulkers E, Oates S, Osborne JP (2017) Swift observations of V404 Cyg during the 2015 outburst: X-ray outflows from super-Eddington accretion. MNRAS 471:1797–1818, DOI 10.1093/mnras/stx1699, 1707.01076

Piirola V (1973) A double image chopping polarimeter. A&A 27:383–388

Piirola V (1988) Simultaneous five-colour (UBVRI) photopolarimeter. In: Coyne GV, Magalhaes AM, Moffat AF, Schulte-Ladbeck RE, Tapia S (eds) Polarized Radiation of Circumstellar Origin, Vatican Observatory/University of Arizona Press, Vatican City State/Tucson, AZ, pp 735–746

Piirola V, Reiz A, Coyne GV (1987) Simultaneous five-colour (UBVRI) polarimetry of EF ERI. A&A 186:120–128

Piirola V, Coyne GV, Reiz A (1990) Simultaneous UBVRI polarimetry of VV Puppis during an active phase. A&A 235:245–254

Piirola V, Scaltriti F, Coyne GV (1992) Circumstellar disks deduced from sub-arcsecond polarization observations of two young stars. Nature 359:399–401, DOI 10.1038/359399a0

Piirola V, Hakala P, Coyne GV (1993) The discovery of variable polarization over the 13.9 minute spin period of the intermediate polar RE 0751 + 14. ApJ 410:L107–L110, DOI 10.1086/186891

Piirola V, Vornanen T, Berdyugin A, Coyne GV, J S (2008) V405 Aurigae: A High Magnetic Field Intermediate Polar. ApJ 684:558–568, DOI 10.1086/590144, 0805.4289

Piirola V, Berdyugin A, Berdyugina S (2014) DIPOL-2: a double image high precision polarimeter. In: Ground-based and Airborne Instrumentation for Astronomy V, Proc. SPIE , vol 9147, p 91478I, DOI 10.1117/12.2055923

Potter SB, Buckley DAH (2018) Time series photopolarimetry and modelling of the white dwarf pulsar in AR Scorpii. MNRAS 481:2384–2392, DOI 10.1093/mnras/sty2407, 1809.01884

Potter SB, Buckley DAH, O'Donoghue D, Romero-Colmenero E, O'Connor J, Fourie P, Evans G, Sass C, Crause L, Still M, Butters OW, Norton AJ, Mukai K (2010) Polarized QPOs from the INTEGRAL polar IGRJ14536-5522 (=Swift J1453.4-5524). MNRAS 402:1161–1170, DOI 10.1111/j.1365-2966.2009.15944.x, 0911.1198

Rodriguez J, Cadolle Bel M, Alfonso-Garzón J, Siegert T, Zhang XL, Grinberg V, Savchenko V, Tomsick JA, Chenevez J, Clavel M, Corbel S, Diehl R, Domingo A, Gouiffès C, Greiner J, Krause MGH, Laurent P, Loh A, Markoff S, Mas-Hesse JM, Miller-Jones JCA, Russell DM, Wilms J (2015) Correlated optical, X-ray, and

γ-ray flaring activity seen with INTEGRAL during the 2015 outburst of V404 Cygni. A&A 581:L9, DOI 10.1051/0004-6361/201527043, 1507.06659

Serkowski K (1974) Polarization techniques. In: Carleton NP (ed) Astrophysics. Part A: Optical and infrared, Academic Press, New York, pp 361–414

Słowikowska A, Krzeszowski K, Zejmo M, Reig P, Steele I (2016) Calibration of the Liverpool Telescope RINGO3 polarimeter. MNRAS 458:759–771, DOI 10.1093/mnras/stw309, 1602.02105

Strassmeier KG, Ilyin I, Järvinen A, Weber M, Woche M, Barnes SI, Bauer SM, Beckert E, Bittner W, Bredthauer R, Carroll TA, Denker C, Dionies F, DiVarano I, Döscher D, Fechner T, Feuerstein D, Granzer T, Hahn T, Harnisch G, Hofmann A, Lesser M, Paschke J, Pankratow S, Plank V, Plüschke D, Popow E, Sablowski D (2015) PEPSI: The high-resolution échelle spectrograph and polarimeter for the Large Binocular Telescope. Astronomische Nachrichten 336:324, DOI 10.1002/asna.201512172, 1505.06492

Veledina A, Berdyugin AV, Kosenkov IA, Kajava JJE, Tsygankov SS, Piirola V, Berdyugina SV, Sakanoi T, Kagitani M, Kravtsov V, Poutanen J (2019) Evolving optical polarization of the black hole X-ray binary MAXI J1820+070. A&A, in press 1808.09002

Vornanen T, Berdyugina SV, Berdyugin AV, Piirola V (2010) GJ 841B — the Second DQ White Dwarf With Polarized CH Molecular Bands. ApJ 720:L52–L55, DOI 10.1088/2041-8205/720/1/L52, 1008.3903

Wiktorowicz SJ, Matthews K (2008) A High-Precision Optical Polarimeter to Measure Inclinations of High-Mass X-Ray Binaries. PASP 120:1282, DOI 10.1086/595966, 0810.5561

Wiktorowicz SJ, Nofi LA (2015) Simultaneous Linear and Circular Optical Polarimetry of Asteroid (4) Vesta. ApJ 800:L1, DOI 10.1088/2041-8205/800/1/L1, 1412.6117